Nanotechnology Perceptions
ISSN 1660-6795
www.nano-ntp.com

Improving Heat Transfer Efficiency in Shell-and-Tube Heat Exchangers through the Incorporation of Alkaline Water Nanofluids

Mohd Majid[1], S.Irudayaraj[2], Melvin Victor De Poures[3*], Arasu Raman[4], S.Venugopal[5], S.Vanitha[6], A.Venkatesh[7], Asha PK[8], S.Baskar[9]

[1]Associate Professor, Department of Mechanical Engineering, Sant Longowal Institute of Engineering and Technology, Longowal 148106, mohdmajid@sliet.ac.in
[2]Professor, Mechanical Engineering, Vel Tech Rangarajan Dr. Sagunthala R&D Institute of Science and Technology, Avadi, Chennai - 600062. drirudayaraj@veltech.edu.in
[3]Associate Professor, Saveetha School of Engineering, Saveetha Institute of Medical and Technical Sciences, SIMATS, Chennai, Tamil Nadu, India, Pincode:602105, melvinvictordepoures.sse@saveetha.com*
[4]Associate Professor, Faculty of Business and Communications, INTI International University, Putra Nilai, 71800, Malaysia, arasu.raman@newinti.edu.my
[5]Assistant Professor, Department of Automobile Engineering, Vels Institute of Science, Technology & Advanced Studies, Chennai - 600117, venugopal.se@velsuniv.ac.in
[6]Assistant Professor, School of Civil Engineering, Sathyabama Institute of Science and Technology, Chennai, India, vanitha.civil@sathyabama.ac.in
[7]Professor & Head of the Department of,Sree Balaji Dental College & Hospital, Dept. of Conservative Dentistry & Endodontics, Bharath Institute of Higher Education & Research (BIHER), Chennai 600 100, denvenkat@gmail.com.
[8]Assistant Professor, Department of Chemistry, New Horizon college of Engineering, ashapkind@gmail.com
[9]Research Fellow, INTI International University, Malaysia, Assistant Professor, Department of Automobile Engineering, Vels Institute of Science, Technology & Advanced Studies, Chennai - 600117, baskar133.se@velsuniv.ac.in

This investigation aimed to experimentally assess the operational efficiency of a shell-and-tube heat exchanger utilizing nanofluids containing Magnesium oxide nanoparticles and alkaline water (MgO-AW), as well as Manganese dioxide and alkaline water (MnO2-AW). The nanofluids, comprising unsurface-modified MgO-AW and MnO2-AW nanoparticles, underwent synthesis. The

study involved analyses to evaluate the impact of varied volume concentrations of nanoparticles on crucial parameters such as thermal conductivity, viscosity, heat transfer coefficient, friction factor, Nusselt number, and pressure drop. The distinctive inherent properties of the nanoparticles resulted in the observation that introducing MgO and MnO2 nanoparticles at a concentration of 0.1 weight percent led to a 29% and 39% increase in the thermal conductivity of the nanofluids, respectively, as indicated by the experimental findings. Moreover, the convective heat transfer coefficient experienced enhancement due to the improved thermal conductivity of the two-phase mixture. Additionally, the friction factor exhibited an increase due to simultaneous rises in both the viscosity and density of the nanofluids. Furthermore, when comparing the MgO nanofluid with the MnO2 nanofluid, it was noted that the latter displayed a significantly reduced pressure drop. This phenomenon can be attributed to the augmentation of the thermophysical properties of the nanofluid.

Keywords: Clean Energy, Sustainable Industry, Climate Action, Consumption and Production, Innovation and Infrastructure.

1. Introduction

Enhancing heat transfer efficiency in industrial applications [1,2] poses a significant challenge for advancing energy-efficient technologies. Various systems, such as engines, fuel cell technology, high-speed electronic components, superconductive magnets, high-flux photonic devices, X-ray equipment, and lasers, require efficient cooling to ensure optimal performance and safety. Despite their small size and high power-to-weight ratio, the heat load in these applications can exceed 2000 W/cm^2. Prioritizing efficiency over adding more heat sources or implementing additional systems like oil radiators and intercoolers is crucial for improving heat transfer equipment efficiency. The introduction of extra heat sources and equipment may lead to increased expenses, space constraints, and environmental impact due to the emission of pollutants like NOx from diesel-fueled vehicle exhaust [3]. Alternative strategies to achieve improved efficiency involve the use of heat transfer fluids that are cost-effective, energy-efficient, and environmentally friendly [4,5]. The refinement of heat exchanger design has focused on hydraulic layout and thermodynamic efficiency [6,7], addressing performance through approaches such as lowering operating temperatures [8], utilizing fouling-resistant materials, and modifying heat- and material-transfer surfaces [9]. The literature also proposes effective techniques for heat exchanger maintenance planning [10]. Adopting these strategies not only enhances heat transfer efficiency but also contributes to cost savings, energy conservation, and environmental sustainability. Low thermal conductivity is prevalent in heat transfer fluids. This shows the rising need for heat-transmitting fluids. Developing high-efficiency heat transport systems like the one discussed requires understanding thermo-fluid properties. Maxwell initially dispersed micrometer-sized particles in 1873 [11]. However, maintaining dispersion stability throughout nanofluid production and use is crucial. Current study has not determined nanoparticles' long-term performance in nanofluids [12]. Numerous studies have shown that nanofluids improve heat transmission. Most studies show that nanofluids boost heat transfer, with just a little pressure drop [13-15].

The utilization of shell-and-tube heat exchangers for heat transfer is prevalent in chemical and petroleum industries. These devices house tube bundles, and researchers from various

academic institutions have delved into studying their efficacy [16]. In a study by Esfahani and Languri, graphene oxide nanofluid was tested for heat transfer in shell-and-tube heat exchangers, revealing that purified water exhibited higher energy loss compared to graphene oxide nanofluid [17].Gao et al. [18] conducted a geometry analysis, uncovering 26% thicker walls than predicted. The simulated flow exhibited a continuous eccentric trajectory, suggesting spin in the heat converter. Yang et al. [19] investigated the impact of graphite nanofluid on the convective heat transfer coefficient in a laminar flow horizontal tube heat exchanger, noting that Reynolds number and volume concentration contributed to increased convective heat transfer.Heris et al. [20-21] observed that Al_2O_3 and CuO nanofluids enhanced circular tube convective heat transfer while maintaining wall temperature. The study emphasized the role of particle volume percentage and Peclet number as enhancers. Li and Xuan [22,23] demonstrated the superior convective heat transfer performance of Cu/water nanofluid compared to the base fluid.Duangthongsuk and Wongwises [24,25] found that 0.2 vol% TiO_2/water nanofluid increased convective heat transport by 6-11%, accompanied by a pressure drop compared to the base fluid. Chandrasekar et al. [26] highlighted a 12.24% enhancement in Nusselt number with 0.1 vol% nanoparticles in Al_2O_3/H_2O nanofluid. Pantzali et al. [27] achieved an 18% improvement using 4 vol% nanoparticles in CuO/H_2O nanofluids.

Farajollahi et al. [28] investigated the impact of Al_2O_3 and TiO_2 water nanoflakes on heat transfer rates in a shell-and-tube heat exchanger, reporting performance improvements ranging from 19% to 56%. Shahrul et al. [29] tested various nanofluids and mass flow rates in a shell-and-tube heat exchanger, with Al_2O_3-Water exhibiting the greatest heat transfer rate at 50 kg min^{-1} mass flow.Lotfi et al. [30] utilized MWNT-water nanofluids to enhance heat transmission in a shell-and-tube heat exchanger, finding that MWNT outperformed the base fluid in heat transmission. These studies collectively contribute to our understanding of nanofluid applications in improving heat transfer efficiency within shell-and-tube heat exchangers.

Nanofluids have been identified in research as enhancers of heat transfer rates, efficiency, entropy, and exergy. The effectiveness of nanofluids hinges on factors such as nanoparticle combination, concentration, size, and external modification. Utilizing the Life Cycle Assessment (LCA) as a robust method for evaluating environmental impacts, stakeholders can gain essential insights for technical, economic, and political comparisons across diverse industrial production sectors. Contrary to existing literature, no comprehensive studies have integrated experimental investigations, nanofluids, and assessments of heat exchanger tubes and shells, particularly in the context of shell-and-tube heat exchangers. Prior research lacked comparisons among these types of heat exchangers and neglected to consider potential reductions in heat exchanger area resulting from an increase in the nanofluid's heat transfer coefficient. To bridge these gaps, this study focuses on examining the effectiveness of MgO-AW and MnO_2-AW nanofluids. The primary goal is to quantify the physical and thermal characteristics of the substance, along with its suspension stability in alkaline water (AW). This necessitates employing various pH levels and surfactant types during nanofluid preparation.Subsequently, the nanofluid, formulated with different volume fractions, is introduced into a Shell-and-Tube Heat Exchanger. The subsequent step involves determining the overall heat transfer coefficient and comparing it with the reference scenario of operation using only distilled water. The obtained trial results are then juxtaposed with a comprehensive

theoretical framework, and an analysis is conducted to explore any deviations from the anticipated performance. This approach aims to fill existing research gaps and provide a holistic understanding of nanofluid behavior in the context of shell-and-tube heat exchangers.

2. Preparation of Nanofluids

The nanofluid comprised 99.5% pure MgO-AW particles with a width of 20 nm. Following manufacturing, these particles were dispersed in alkaline water. The nanofluid was prepared with volume fractions of 0.05%, 0.1%, and 0.15%, calculated from volumetric data. The objective was to address fluid adherence issues and stabilize surfaces through pH adjustments and the use of SDS surfactant, ensuring the creation of durable nanofluids with the required dispersion fractions of nanoparticles.Ultrasonic homogenization (Hielscher UP300St, 500 W, 30 kHz) for either 60 or 120 minutes at 70% amplitude proved effective in better disseminating nanoparticles in the base fluid. The nanofluid's hydrodynamic size distribution and potential were evaluated using a Zeta sizer. Temperature variations from 25 to 70 degrees Celsius were considered, with continued trials at 5 degrees Celsius to minimize air and moisture contamination and enhance data reliability.Digital viscometers precisely measured the viscosity at 0.5%, while the falling ball technique, employing a 1.59-millimeter capillary tube, achieved the desired accuracy. Peltier devices were utilized to regulate capillary temperature with a precision of 0.01 Kelvin, resulting in a 1% deviation in viscosity. Thermal properties analyzers, estimating nanofluid thermal conductivity within 5%, introduced a predicted 5% error.All measurements were completed in a brief duration of 1 minute and 10 seconds. Nanofluid samples were stored in septum containers, and a 25-ml vial with a circumference of 20mm was employed. The sensor syringe probe, submerged and positioned vertically and centrally in the vial, eliminated probe-vial wall contact, ensuring the avoidance of uncontrolled convection errors and the attainment of accurate results. To guarantee precision, samples were thermally equilibrated at various temperatures for 15 minutes before analysis.The study's thermocouples and flow meter exhibited an accuracy level of 2.2%, contributing to the overall reliability of the experimental setup.

2.1Preparation and stability characterization

Field supplier MatLab supplied the MgO-AW nanoparticles utilized in this study. All subject-related data is in Table 1. A two-step process using alkaline water produced MgO-AW nanofibers. The base fluid was formulated using pH values 2, 8, 10.5, 13, 10 in the first step of the experiment. Using exact amounts of HCl, KOH, and NaOH created a variety of pH values. MgO-AW nanoparticles at.05,.10, and.15 vol% were added to the base fluid.[Table 2]. To account for expected particle aggregation and sedimentation, the same amount (0.05 vol%) was tested at different pH levels (2, 8, 10.5, 13, and 10) without the surfactant. To determine how the SDS surfactant affects NF solidity, it is subjected to equal pH values (2, 8, 10.5, 13, and 10). Figure 1 depicts nanofluid arrangement. The technique includes measuring nanofluid pH, homogenizing and sonication, measuring size and zeta, and assessing final features. Hydrodynamic dimensions and zeta potential were measured at room temperature. Sedimentation and aggregation considerably affect nanofluid (NF) stability and effectiveness [32]. A lot of study is being done to mitigate these two issues [33]. After manufacturing, the nanofluids were examined visually for temporal stability.

Table 1. Basefluid and nanoparticle physical attributes

Properties	Unit	Alkaline Water	MgO	MnO_2
Heat capacity	$J.kg^{-1}.K^{-1}$	4879	635.8	628.8
Density	$kg.m^{-3}$	967.1	6880	7820
Thermal conductivity	$Wm^{-1}.K^{-1}$	0.813	78.5	79.5
Thermal expansion coefficient	K^{-1}	2.9×10^{-4}	1.66×10^{-5}	1.77×10^{-5}
Dynamic viscosity	$Ns.m^{-2}$	0.001233	0.0019	0.0021

Table 2.NF continuity in zeta potential and sonication time in both cases, with and devoid of a surfactant

Specimen	Surface-Active Agent	pH Pre/Post-Sonication	Sonication time (h)	Zeta potential (mV)	Particle Dimensions (nm)	Comments
1	None	2.00/8.23	1	28.9	50nm	pH:unstableZeta:acceptable
2	None	8.40/9.71	1	−29.8	46nm	pH:stableZeta:acceptable
3	None	12.00/13.66	1	−10.6	40nm	pH:stable Zeta: low
4	SDS 0.2 m	12.00/7.96	1	−13.8	35nm	pH:stable Zeta: low
5	SDS 0.2 m	11.50/12.9	2	19.1	30nm	pH:stable Zeta: low
6	None	2.12/2.7	2	31.5	20nm	pH:stable Zeta: good

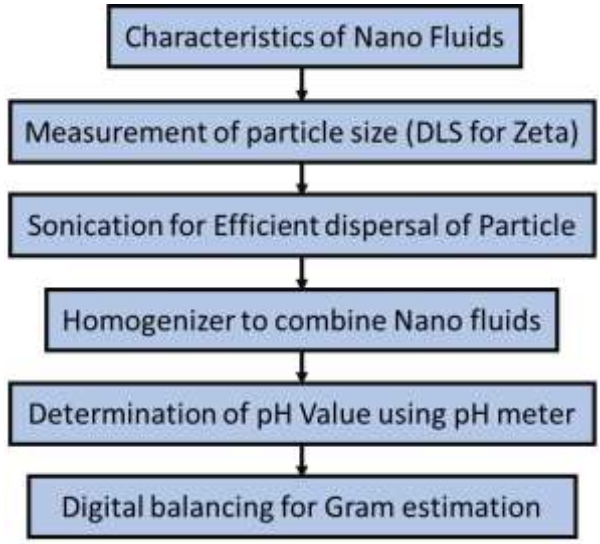

Fig. 1. NFs production and property measurement process

2.2 Effect of pH

In Figure 2, it is evident that pH 8.5 exhibits the highest zeta potential at 29.8 mV, followed closely by pH 2 with a zeta potential of 28.9 mV. Zeta potentials at pH 11 and 13 are comparatively lower at 10.6 and 13.8, respectively. The interaction of nanoparticles in aqueous solutions with pH values of 8.5, 2, 11, and 13 led to changes in the base fluid's pH to 9.81, 8.76, 8.96, and 11.66. This alteration occurred during the sonication process of nanoparticles. Referring to Chang et al. [34], the isoelectric temperature of nanofluids was found to be at pH 10. Consequently, the researchers determined that a pH of 6.5 would provide their nanofluids with optimal endurance. Surprisingly, the samples in this study exhibited the highest stability values in comparison to existing literature. This was discerned by comparing the results with

prior publications. In a different investigation where pH was adjusted to 10.2, persistent nanofluid suspensions were created without the use of surfactants. Even after one hour of sonication at 0.4 vol%, these suspensions remained stable for 45 days. Notably, achieving this stability was accomplished without employing any surfactants. The pH of both the liquid and the solid phase, including the isoelectric point and boiling point, plays a crucial role in determining nanoparticle charge polarity. The higher density of charges per unit area on the surface results in increased repulsive forces [35], effectively preventing particle aggregation.

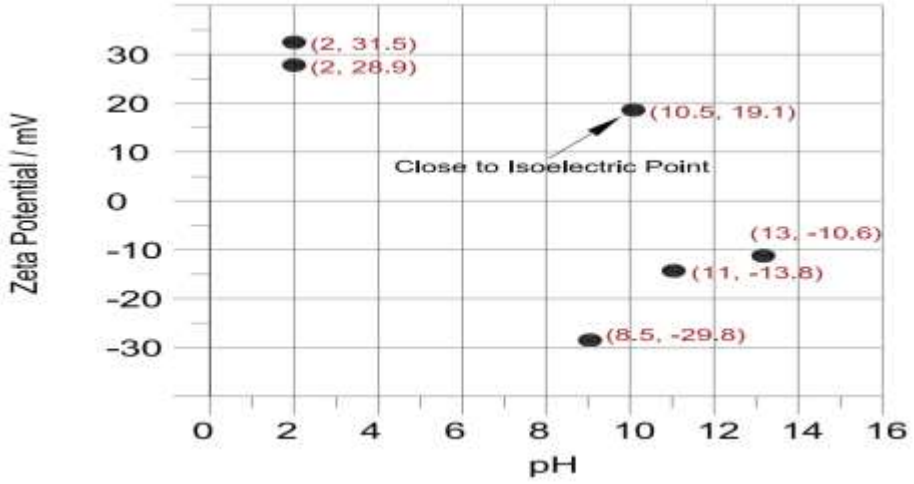

Fig. 2. Effect of pH on zeta potential value.

2.3 Effect of surfactant

Surfactants play a crucial role in stabilizing nanoparticles in fluid suspensions [36]. In Figure 3, the impact of nanofluid stability with 0.05% surfactant is illustrated. The research investigated how varying sonication times influenced experimental outcomes, along with the effects of four different pH levels on nanofluids (NFs) with identical volume fractions. Multiple experiments were conducted considering the use of surfactants, with SDS being the surfactant of choice in this study. After one hour of sonication at pH 12, the zeta potential increased from 12.5 to 19.8 mV. At pH 10, there was minimal improvement, while the zeta potential value decreased from 24.4 mV to 2.86 mV after two hours of sonication at pH 2. Conversely, at pH 11.5, the zeta potential rose from 0.0763 to 11 mV. The selection of surfactants is crucial, as their capacity to interact with both the base fluid and nanoparticles significantly influences their effectiveness. It is noteworthy that the nanofluid containing SDS showed less improvement compared to the surfactant-free nanofluid. As a result, the research focused on surfactant-free nanofluid exploration.

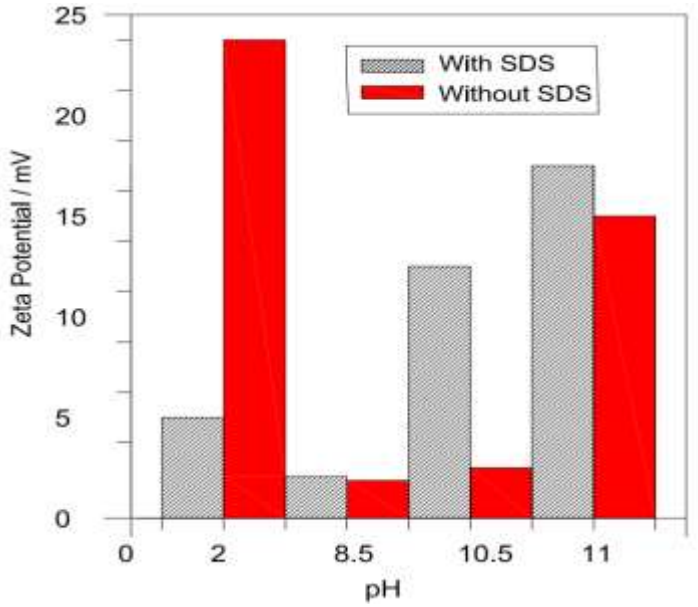

Fig.3.The impact of varying sonication durations on zeta potential value

3. Experimental Setup.

In Figure 4, both a schematic illustration and a photograph of the shell-and-tube heat exchanger employed in this experiment are presented. Further specifications of the heat exchanger are detailed in Table 3, located below the aforementioned visuals. The shell of the heat exchanger was dedicated to circulating cold water, while the tube facilitated the circulation of hot nanofluids, utilizing both components of the heat exchanger. Throughout the experimental study, a diverse range of volume concentrations of nanoparticles was explored, coupled with various mass flow rates. The two barrels were primarily filled with the required solutions at a predefined temperature. Thermocouples were integrated into the data collection apparatus to precisely measure the temperature of liquids with varying degrees of warmth. The temperatures of both inflowing and outflowing fluids were meticulously monitored while adjusting the volume concentration of nanoparticles. The heat temperatures displayed a broad range, encompassing both high and low values. These temperatures were compared for the purpose of analysis and assessment. A simplified dynamic heat exchanger model was utilized to calibrate heat transfer correlations for both the tube side and the shell side. This dynamic model, as introduced by Correa and Marchetti [37], is a distributed parameter model featuring small Control Volumes (CVs), each representing a lumped parameter counter-flow heat exchanger model. The model takes into account the thermal capacitance of the tube bundle while neglecting that of the shell metallic parts. Additionally, it assumes no pressure loss at either the shell side or the tube side, resulting in equal inlet and outlet mass flow rates.

(a)

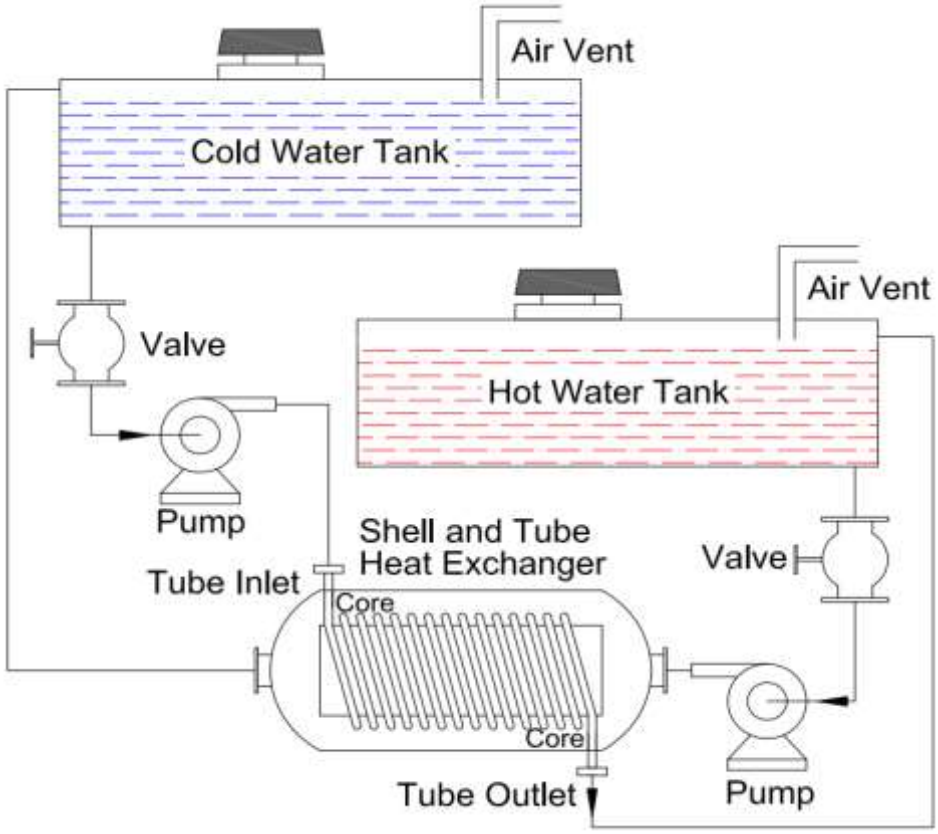

(b)

Fig. 4. a).Photographic view of shell and tube Exchanger b) A shell and tube heat exchanger schematic

Table 3.Heat exchanger shell and tube specifications

Details	Dimensions (mm)
Number of tubes	16
Shell length	900
Shell diameter	225
Internal Tube Diameter	15
External Tube Diameter	18

4. Thermophysical properties of nanofluids

The thermal mobility of the nanofluid must be determined immediately to ensure mathematical predictions match real results. Nanofluid thermophysical properties are determined using the H-C model [38]. This model is used to calculate fluid thermal conductivity in many applications.

$$k_{nf} = \left[\frac{k_p+(m-1)k_t-(m-1)\emptyset(k_t-k_p)}{k_p+(m-1)k_t+\emptyset(k_t-k_p)}\right]k_t \quad (1)$$

Thermal conductivity may assess spherical particles' direct proof form factor N and degree of sphericity. Two traits distinguish spherical particles. This is the sole option for object sphericity. Nanoparticle and base fluid thermal conductivity is denoted by knf and kp. Nanoparticles have far higher thermal conductivity than base fluids. The mathematical model created by Dr. Bruggeman is: Murshed et al. measured nanofluid thermal conductivity [39].

$$k_{nf} = 0.25\left[(3\emptyset-1)k_p + (2-3\emptyset)k_t\right] + \frac{k_t}{4}\sqrt{\Delta} \quad (2)$$

$$\Delta = \left[(3\emptyset-1)^2\left(\frac{k_p}{k_t}\right)^2 + (2-3\emptyset)^2 + 2(2+9\emptyset-9\emptyset^2)\left(\frac{k_p}{k_t}\right)\right] \quad (3)$$

In their study, Yu and Choi (40) developed a new mathematical equation for calculating thermal conductivity. The equation is presented below:

$$k_{nf} = \left[\frac{k_p + 2k_t - 2\emptyset(k_t-k_p)(1+\beta)^3\emptyset}{k_p + 2k_t + \emptyset(k_t-k_p)(1+\beta)^3\emptyset}\right]k_t \quad (4)$$

where β is the ratio of nanolayer thickness to particle radius. A nanofluid's thermal efficiency is typically determined using b = 0.1.Timofeeva et al. [41] pioneered the effective medium method for computing nanofluid thermal conductivity.

$$k_{nf} = [1+3\emptyset]k_t \quad (5)$$

By employing one of the multiple theoretical approaches at our disposal, it becomes possible to determine the heating capacity of microfluidics. The consistency of a nanofluid is a crucial parameter that significantly influences the nanofluid's performance. This study aims to examine the predictive capabilities of established models and subsequently compare their

predictions with the actual findings. Batchelor [42] proposes the utilization of a straightforward equation for the calculation of fluid viscosity that incorporates spherical nanoparticles.

$$\mu_{nf} = (1 + 2.5\emptyset + 6.2\emptyset^2)\mu_t \quad (6)$$

Drew and Passman [43] present an equation based on the Einstein field theory that may be used to calculate the spherical particle viscosity with volume.

$$\mu_{nf} = (1 + 2.5\emptyset)\mu_t \quad (7)$$

Brinkman [44] Einstein's equation has been simplified to the following mathematical structure:

$$\mu_{nf} = \frac{1}{(1-\emptyset)^{2.5}}\mu_t \quad (8)$$

A model for determining the nanofluid viscosity was suggested by Wang et al. [45], and it may be summarized as follows:

$$\mu_{nf} = (1 + 7.3\emptyset + 123\emptyset^2)\mu_t \quad (9)$$

where Φ is the molecular volumetric fixation, μnf is the nanofluid's consistency, and t is the amount of thickness of the therminol or base liquid.

For the purpose of analysis, each measurement was repeated three times, and the average of these three sets of results was used to determine the best course of action moving forward. On the other hand, the specific heat may be easily determined by applying Equation (10) [46] to the data.

$$C_{nf} = \frac{(1-\varphi)(\rho C)_{bf} + \varphi(\rho C)_{np}}{\rho_{nf}} \quad (10)$$

The coefficient for convective heat transfer was determined by employing the equation of Newton's of cooling as the fundamental principle for the calculation. The heat transfer from the hot nanofluid to the cold water is equivalent to the heat absorption by the water. The convective transfer of heat coefficient, Nusselt number, and friction factor were determined through calculations using experimental data. The thermal and physical parameters utilized for theoretical computations are outlined in tables 4 and 5.

The convective heat transfer coefficient is calculated using Newton's cooling law.

$$q = hA\Delta Tm = mC(Tc,o - Tc,i) \quad (11)$$

Nanofluid number according to the Nusselt scale

$$Nu_{nf} = hd/k \quad (12)$$

Nanofluid's coefficient of internal friction

$$F_{nf} = \frac{p}{\left(\frac{L}{D}\right)\left(\frac{\rho V}{2}\right)} \quad (13)$$

Density of nanofluid $\rho_{nf} = (1-\Phi)\rho_f + \rho_p\Phi$ (14)

Table 4. shows the thermophysical characteristics of the fluids in the tube side at 25 °C and the fluid in the shell side at 80 °C.

Nanofluid in Tube Section		Water in Shell Section
0.76	Heat Conductance (Wm−1 .K−1)	0.796
0.00205578	Fluid Resistance (kg.m−1 .s−1)	0.0002786
1000	Mass Density (kg.m−3)	998
5120	Heat Capacity (J.kg−1 .K−1)	4500

Table 5. Inputs for calculations involving heat transfer

Label (Measurement Unit)	Numerical Reading
k of Tube Material (W.m−1 .K−1)	64
Individual Tube and Shell Length (meters)	0.26
F_b	0.3
N_b	9
Aggregate Tube Length (meters)	6.5
Diameter of Particles dp (nanometers)	20
Percentage of Volume Fraction	0.05
Tube Spacing - p	0.0085
Inter-Baffle Gap - P	0.0276

5. Results and Discussion

5.1 Thermal Conductivity.

Supplementary Figure 5 depicts changes in nanofluid thermal conductivity at 30°C, revealing an increase as nanoparticles per unit volume rise. The investigation provides insights based on volume-based percentages, highlighting that the thermal conductivity of the nanofluid elevates with an increase in nanoparticles and distilled water content. This observed trend underscores the influence of both the unique inherent properties of nanoparticles and their size, shape, and aspect ratio on the composite material's thermal conductivity [47]. Notably, there is a linear correlation between thermal conductivity and volume percentages, a trend consistent with findings from previous studies by Jiang et al. [48] and Halelfadl et al. [49]. Moreover, Supplementary Figure 5 highlights a substantial difference in thermal conductivity between the MnO_2 nanofluid and the MgO nanofluid, with the former exhibiting significantly higher thermal conductivity.

The thermal conductivity of nanofluids and alkaline water was assessed at 30°C. Supplementary Figure 6 illustrates that thermal conductivity experiences an increase with an escalation in nanoparticle volume percentage. To delve deeper into this enhancement, nanofluids were compared to alkaline water at comparable temperatures. The figure demonstrates that the thermal conductivity of MgO and MnO_2 nanofluids rises in tandem with increasing nanoparticle volume percentages. Specifically, at a 0.1% volume percentage, MgO and MnO_2 nanoparticles in distilled water led to a respective increase in thermal conductivity by 29.9% and 40.6%. This study concludes that the addition of nanoparticles to distilled water results in an augmented thermal conductivity, attributed to phenomena such as Brownian motion and efficient heat transfer [50]. Moreover, the thermal conductivity increase observed in MnO_2 nanofluids surpasses that of MgO nanofluid, elucidating that the inherent properties of MnO_2 nanoparticles contribute to their higher thermal conductivity.

5.2 Convective Heat Transfer Coefficient.

When the Reynolds number is changed, Magnesium oxide (MgO) and Manganese dioxide (MnO_2) nanofluids' coefficients of convective heat transfer vary. The convective heat transfer coefficient varies for nanoparticle solutions in these Supplementary figures 7(a) and (b). The results indicate that the coefficient of convective heat transfer increases proportionately with nano-particle amounts, independent of their properties. The two-phase combination's increased heat conductivity may explain it. Due to nanoparticle Brownian motion, RE number increases convective heat transmission. A higher RE number increases nanoparticle displacement, speeding energy transfer in nanofluids. Researchers examined the convective heat transfer coefficient in isothermal circumstances with different Reynolds numbers. Figure 7(c) shows the RE number-convective heat transfer coefficient connection. Especially with water at 50 degrees Celsius, a nanofluid with a volume fraction of 0.15 has this connection. Alkaline water and nanofluids have higher heat transfer coefficients as Reynolds numbers rise. At a specific Reynolds number, carbon nanotube (MnO_2) nanofluid has a higher heat transfer coefficient than silicon carbide (MgO).

5.3 Friction Factor.

Supplementary Figures 8(a) and 8(b) provide a comparative analysis of the friction factor and Reynolds number for MgO nanofluids and MnO_2 nanofluids. These figures systematically explore a broad range of nanoparticle volume concentrations, shedding light on the intricate interaction between these variables. The experiments reveal that as the Reynolds number increases, the friction factor decreases for both nanofluids. The alteration in nanoparticle concentration within the fluid leads to changes in viscosity and density, subsequently influencing the friction factor. This phenomenon is a consequence of the nanoparticles altering the fluid properties. In Figure 8(c), an intriguing curve illustrates the complex relationship between the friction factor and Reynolds number, particularly focusing on the impact of 0.15% volume concentrations of nanoparticles in MgO and MnO_2 nanofluids. The curve highlights that the coefficient of friction rises in tandem with the increase in the Reynolds number, demonstrating a clear correlation. The rise in nanoparticle concentration contributes to an increase in nanofluid viscosity and density. As nanoparticles become more prevalent in the solution, the friction factor experiences an upward trend. This increase in viscosity correlates with a corresponding rise in density. The elevated density diminishes the translational flexibility of nanoparticles, leading to an increase in the friction factor [51]. It is noteworthy that the friction factor of carbon nanotube (MnO_2) nanofluids significantly surpasses that of silicon carbide (MgO) nanofluids. This difference in viscosity and density between MnO_2 nanofluid and MgO nanofluid could potentially account for the observed distinction in the friction factor.

5.4 Viscosity.

Supplementary Figure 9 depicts the relationship between viscosity and volume fraction, with both parameters measured at standard room temperature. A discernible trend is observed wherein the viscosity of the liquid increases as the volume fraction grows. This escalation is attributed to the deposition of more nanoparticles in the fluid. The nanoparticles act as obstacles to fluid flow, impeding its movement. Notably, the viscosity of the MnO_2 nanofluid is significantly higher than that of the MgO nanofluid due to the higher mass density of MnO_2

nanoparticles.

5.5 Nusselt Number.

The relationship between the Nusselt number (Nu) and the Reynolds number (Re) for different ratios of SiC and MnO_2 nanoparticles is illustrated in Supplementary Figure 10(a) and Supplementary Figure 10(b) respectively. Robust evidence has consistently demonstrated a strong positive correlation between the Nu number and the concentration of nanoparticles. This correlation appears to resemble a linear connection, highlighting the direct impact of an increasing amount of nanoparticles on the Nu number. Several factors may contribute to the observed increase in the Nu number, including the Brownian motion of nanoparticles, reduction of the edge layer, and an elevation in the resistance factor [52]. Figure 10(c) further illustrates the correlation between the Nusselt number and the Reynolds number, specifically focusing on the scenario with a nanoparticle concentration of 0.15 volume percentage. The Nu number exhibits a linear relationship with the Re number, as depicted in the figure. Notably, the MnO_2 nanofluid demonstrates a higher Nu number compared to the MgO nanoparticles. This observation is attributed to the higher thermal conductivity of MnO_2 nanoparticles in comparison to MgO nanoparticles. The findings align with previous research conducted by numerous researchers [53,54].

5.6 Pressure Drop.

The relationship between variations in pressure drop and Reynolds number is illustrated in Supplementary Figures 11(a)–11(c). It is observed that an increase in the Reynolds number corresponds to a rise in pressure loss, regardless of the specific type of nanofluid under consideration. This phenomenon is likely associated with the enhancement of the thermophysical attributes of water resulting from the introduction of nanoparticles into distilled water. Consequently, the heat exchanger experiences an elevated pressure drop due to this effect [55-58]. The pressure drop induced by the MgO nanofluid is notably greater compared to the MnO_2 nanofluid. For instance, at a Reynolds number (Re) of 5000 and a nanoparticle volume fraction of 0.14, nanofluids containing carbon nanotubes (MnO_2) nanoparticles and silicon carbide (MgO) nanoparticles exhibited pressure drops of 7.8 kPa and 6.2 kPa, respectively. This observation remained consistent despite the low nanoparticle volume fraction of only 0.14. Compared to the pressure drop caused by pure water, the detected pressure drop indicates an initial increase of 40%, followed by an additional 30% increase.

5.7Area reduction

The temperature at the outflow of the system is shown in Supplementary Figure 12, which may be accessed at the following location. The temperature gradients of both hot and cold fluids at different levels and flow rates are shown in Supplementary Figures 13(a) and 13(b), respectively. Based on the graphical representations, it can be shown that when the MnO_2 /A nanofluid's flow rate rises, A similar rise in the temperature decrease for the hot fluid at the output occurs. In contrast, under these circumstances, the cold fluid's temperature rises. The observed trend in the temperature profile may be attributed to the enhanced heat transfer features of the Manganese dioxide / Magnesium oxide nanoparticle nanofluid.

Reynolds number (Re) characterizes system flow. Based on velocity, Reynolds number was

computed. Supplementary Table 6 volume concentration indicated a 4.67% lower Reynolds number for the Nanofluid/Water combination due to the higher viscosity of the Manganese dioxide / Magnesium oxide nanoparticle nanofluid. As demonstrated in Supplementary table 6, the nanofluid/water system's Nu is 5.27% lower due to lower RE and Prandtl values. Nanofluid/Water convective heat transfer increases 11.39%. Reynolds number indicates system stream. Table 6 shows that the Manganese dioxide / Magnesium oxide nanoparticle nanofluid's higher viscosity lowers the Reynolds number of the Nanofluid/Water mixture by 4.67%. As indicated in Supplementary table 6, the nano-fluid/water system's Nu is 5.27% lower due to lower RE and Prandtl numbers. The Nanofluid/Water system's convective heat transfer coefficient rose 11.39%, indicating no performance loss. The enhanced TC of Manganese dioxide (MnO_2) nanofluid compensated for the drop in Nusselt (Nu), enhancing convective heat transfer. Nanoparticles substantially change tube wall temperature. Nanofluid flow considerably cools tube walls. Rising Reynolds number lowers wall temperature. Heat from the tube barrier to the nanofluid may increase due to this. Surface nanoparticles absorb heat. Nanoparticles reintegrate with bulk fluid, cooling tube walls.

Reynolds number (Re) and mass flow rate are linearly correlated when particle volume percent is constant. Reduced Reynolds value reduces nanofluid Nusselt value. Nanofluids have greater convective heat transfer than base fluids. Solid nanoparticles in the base fluid increase nanofluid viscosity, increasing resistance compared to water. Increased nanofluid viscosity. A nanofluid with 0.05% Manganese dioxide /atomized water has 1% greater friction than water. Previous studies [55,56] yielded similar findings. Increase the fluid's heat transfer coefficient or surface area to improve convective heat transport. Nanofluid may substitute water in heat exchangers to save space and efficiency. Increased convective heat transfer coefficient (hi) reduced thermal resistance and raised U. This 6% increase for the Nanofluid/Water system indicates tremendous progress. With the higher heat transfer coefficient, Nanofluid/Water system heat transfer area decreased 5.9%.

5.8 Life Phase and Economic Assessment

The initial prototype was powered by grid electricity in a life phase investigation. This basic prototype consists of a shell, pipes, tubes, pump, and storage tank. The life phase assessment involved calculating the baseline's 25-year energy consumption, CO_2 emissions, and cost. The operation of the basic prototype requires 3 kW of power, and it is expected to operate for 300 days per year, 12 hours each day, with electrical grid electricity powering the system. The evaluation included an analysis of a selection of materials capable of downcycling or recycling to assess the potential for energy recovery at the end of the product's life. Supplementary Figure 14 presents the results of the life phase research.

The substitution of existing power sources with renewable energy holds the potential to reduce carbon dioxide emissions and minimize environmental impact. Introducing a particle emission control device in the material manufacturing process can effectively mitigate difficult-to-regulate hazardous emissions and their environmental consequences. Environmental studies have indicated the feasibility of energy-efficient and pollution-reducing techniques, emphasizing the importance of concurrently conducting cost analyses and optimizing performance. Despite advancements in research, there remains a gap in the comprehensive examination of nanofluid production expenses, particularly in the context of hydrothermal

optimization studies. Future optimization studies should economically scrutinize nanofluid production costs while considering heat transmission and pressure decrease aspects. In alignment with the preceding paragraph's recommendations, there is a pressing need for in-depth investigations into the economic and environmental implications of nanofluids. Additionally, potential drawbacks of nanoparticles in various applications require careful examination. Establishing industry standards, methodologies, norms, and protocols for nanofluid production and application is crucial for ensuring consistency and quality.

6. Conclusions

This Research presents a comprehensive study evaluating the efficiency of shell and tube heat exchangers, grounded in theoretical analyses and thermodynamic principles. Additionally, a life cycle assessment is conducted for heat exchangers with a shell and tube design. To fulfill the specified objectives, an experimental setup of a solid-liquid heat exchanger (STHX) was constructed to investigate the performance of MgO/AW and MnO_2/AW nanofluids. Ensuring the uniformity of the nanofluid during its application in the heat exchanger involved following a distinct procedure to prepare the nanofluid based on a predetermined protocol. A series of experimental investigations were carried out to evaluate the heat exchanger's effectiveness under various conditions, including different volume percentages of nanoparticles within the nanofluids.

- In comparison to conventional alkaline water, the utilization of MgO and MnO_2 nanoparticles in nanofluids resulted in enhancements of 30% and 39% in thermal conductivity, respectively. The unique inherent characteristic of the nanoparticles was accountable for the achieved enhancement in thermal conductivity

- The convective heat transfer ratio of MgO -AW and MnO_2-AW nanofluids exhibited a significant enhancement of 26% and 42%, respectively, in comparison to Alkaline water, owing to the notable Enhancement in the Thermal Conductivity of the Nanofluids. Furthermore, the friction factor experienced a notable increase of 6% and 10% correspondingly, upon the incorporation of 0.1 weight percent of MgO or MnO_2 nanoparticles into the formulation.

- The increase in viscosity and volume of the nanofluids has led the friction factor to increase. The use of carbon nanotube (MnO_2) nanofluid in the heat exchanger yielded a significant 40% rise in pressure drop, in contrast to the usage of distilled water. The rise in performance may be ascribed to the improved thermophysical characteristics shown by the nanofluid.

- The incorporation of surfactants has been shown to enhance the performance of nanofiltration (NF) systems. On the other hand, it has been shown that a rise in the NFs' volume concentration causes a decline in their stability.

- Ultrasonication plays a vital role in the disruption of nanoparticle aggregation inside a nanofluid. The aforementioned parameter exhibits variability across various sonication durations, hence exerting an influence on the thermal conductivity (TC), stability and viscosity of the nanofluid (NF).

- The outcomes of the study indicate that the release of heat is greater when using NF as a hot or cold stream, in comparison to Alkaline water.

- The total heat transfer coefficient exhibited a 8% increase, while convective heat transfer had an 11.44% increase. Additionally, there was a decrease in the heat exchanger area by 8.33%.

The study showed that shell-and-tube heat exchangers may employ carbon nanotube/alumina-water nanofluids (MnO_2/AW NF). This is due to the nanofluid's thermal conductivity (TC), which improves heat transmission. Life cycle analysis (LCA) evaluates energy emissions from material prices, production processes, and other variables. It also illuminates how these components affect the benchmark prototype system's costs. Making educated judgments and developing efficient systems need this knowledge. Advances will spur nanofluids research and heat exchanger application.

Statement on Data Accessibility

The authors confirm that the paper includes the study's data.

Conflicts of Interest: The authors declare no conflict of interest.

References

1. Khafaji, Hayder QA, Hasanain A. Abdul Wahhab, Sajda S. Alsaedi, Wisam Abed Kattea Al-Maliki, Falah Alobaid, and Bernd Epple. "Thermal performance evaluation of a tubular heat exchanger fitted with combined basket–twisted tape inserts." Applied Sciences 12, no. 10 (2022): 4807.
2. Hasan Ibrahim, Sahira, and Hasanain A. Abdul Wahhab. "Influence of Twisted Tape Inserts with Perforation on Heat Transfer and Pressure Drop Inside Circular Tube: Numerical and Experimental Investigation." In ICPER 2020: Proceedings of the 7th International Conference on Production, Energy and Reliability, pp. 281-293. Singapore: Springer Nature Singapore, 2022..
3. Biswas, Nirmalendu, Nirmal K. Manna, Ali J. Chamkha, and Dipak Kumar Mandal. "Effect of surface waviness on MHD thermo-gravitational convection of Cu− Al2O3− water hybrid nanofluid in a porous oblique enclosure." Physica Scripta 96, no. 10 (2021): 105002..
4. Mebarek-Oudina, F., Preeti, A. S. Sabu, H. Vaidya, R. W. Lewis, S. Areekara, A. Mathew, and A. I. Ismail. "Hydromagnetic flow of magnetite–water nanofluid utilizing adapted Buongiorno model." International Journal of Modern Physics B (2023): 2450003.
5. Mariadhas, Anish, Puneeth Reddy SV, Bency P, Nivin Joy, Sahaya Susmi SK, and Jayaprakash V. "Analyzing the pressure and thermal efficiency of chemically synthesized nanofluids for computer cooling methods." Proceedings of the Institution of Mechanical Engineers, Part E: Journal of Process Mechanical Engineering (2023): 09544089231161471.
6. B Jidhesh, P., T. V. Arjunan, N. Gunasekar, and M. Mohanraj. "Experimental thermodynamic performance analysis of semi-transparent photovoltaic-thermal hybrid collectors using nanofluids." Proceedings of the Institution of Mechanical Engineers, Part E: Journal of Process Mechanical Engineering 235, no. 5 (2021): 1639-1651.
7. Krishna Varma, K. P. V., Kavati Venkateswarlu, P. V. Durga Prasad, and Uday Kumar Nutakki. "Prediction of stability parameters of ferric oxide nanofluids using response surface methodology based on desirability approach." Proceedings of the Institution of Mechanical Engineers, Part E: Journal of Process Mechanical Engineering (2023): 09544089231151541.

8. Hassaan, Amr M. "Evaluation for the performance of heat transfer process in a double pipe heat exchanger using nanofluids." Proceedings of the Institution of Mechanical Engineers, Part E: Journal of Process Mechanical Engineering 236, no. 5 (2022): 2139-2146.
9. Bashtani, Iman, Javad Abolfazli Esfahani, and Kyung Chun Kim. "Effects of water-aluminum oxide nanofluid on double pipe heat exchanger with gear disc turbulators: A numerical investigation." Journal of the Taiwan Institute of Chemical Engineers 124 (2021): 63-74.
10. Karimipour, Arash, Mohammad Hemmat Esfe, Mohammad Reza Safaei, Davood Toghraie Semiromi, Saeed Jafari, and S. N. Kazi. "Mixed convection of copper–water nanofluid in a shallow inclined lid driven cavity using the lattice Boltzmann method." Physica A: Statistical Mechanics and Its Applications 402 (2014): 150-168.
11. Gupta, Munish, Vinay Singh, Satish Kumar, Sandeep Kumar, Neeraj Dilbaghi, and Zafar Said. "Up to date review on the synthesis and thermophysical properties of hybrid nanofluids." Journal of cleaner production 190 (2018): 169-192.
12. Said, Z., M. A. Sabiha, Rahman Saidur, A. Hepbasli, Nasrudin Abd Rahim, Saad Mekhilef, and T. A. Ward. "Performance enhancement of a flat plate solar collector using titanium dioxide nanofluid and polyethylene glycol dispersant." Journal of Cleaner Production 92 (2015): 343-353.
13. Bellos, Evangelos, and Christos Tzivanidis. "Thermal analysis of parabolic trough collector operating with mono and hybrid nanofluids." Sustainable Energy Technologies and Assessments 26 (2018): 105-115.
14. Al-Waeli, Ali HA, Kamaruzzaman Sopian, Hussein A. Kazem, and Miqdam T. Chaichan. "Nanofluid based grid connected PV/T systems in Malaysia: A techno-economical assessment." Sustainable Energy Technologies and Assessments 28 (2018): 81-95.
15. Said, Zafar, Sahil Arora, and Evangelos Bellos. "A review on performance and environmental effects of conventional and nanofluid-based thermal photovoltaics." Renewable and Sustainable Energy Reviews 94 (2018): 302-316.
16. Said, Z., S. M. A. Rahman, M. El Haj Assad, and Abdul Hai Alami. "Heat transfer enhancement and life cycle analysis of a Shell-and-Tube Heat Exchanger using stable CuO/water nanofluid." Sustainable Energy technologies and assessments 31 (2019): 306-317.
17. Esfahani, Milad Rabbani, and Ehsan Mohseni Languri. "Exergy analysis of a shell-and-tube heat exchanger using graphene oxide nanofluids." Experimental Thermal and Fluid Science 83 (2017): 100-106.
18. Gao, Shiming, Shuo Qu, Junhao Ding, Hui Liu, and Xu Song. "Influence of cell size and its gradient on thermo-hydraulic characteristics of triply periodic minimal surface heat exchangers." Applied Thermal Engineering 232 (2023): 121098.
19. Yang, Ying, Z. George Zhang, Eric A. Grulke, William B. Anderson, and Gefei Wu. "Heat transfer properties of nanoparticle-in-fluid dispersions (nanofluids) in laminar flow." International journal of heat and mass transfer 48, no. 6 (2005): 1107-1116.
20. Heris, S. Zeinali, S. Gh Etemad, and M. Nasr Esfahany. "Experimental investigation of oxide nanofluids laminar flow convective heat transfer." International communications in heat and mass transfer 33, no. 4 (2006): 529-535.
21. Heris, S. Zeinali, M. Nasr Esfahany, and S. Gh Etemad. "Experimental investigation of convective heat transfer of Al2O3/water nanofluid in circular tube." International journal of heat and fluid flow 28, no. 2 (2007): 203-210.
22. Li, Qiang, and Yimin Xuan. "Convective heat transfer and flow characteristics of Cu-water nanofluid." Science in China Series E: Technolgical Science 45 (2002): 408-416.
23. Xuan, Yimin, and Qiang Li. "Investigation on convective heat transfer and flow features of nanofluids." J. Heat transfer 125, no. 1 (2003): 151-155.
24. Duangthongsuk, Weerapun, and Somchai Wongwises. "Heat transfer enhancement and pressure drop characteristics of TiO2–water nanofluid in a double-tube counter flow heat

exchanger." International Journal of Heat and Mass Transfer 52, no. 7-8 (2009): 2059-2067.
25. Duangthongsuk, Weerapun, and Somchai Wongwises. "Effect of thermophysical properties models on the predicting of the convective heat transfer coefficient for low concentration nanofluid." International Communications in Heat and Mass Transfer 35, no. 10 (2008): 1320-1326.
26. Chandrasekar, M., S. Suresh, and A. Chandra Bose. "Experimental studies on heat transfer and friction factor characteristics of Al2O3/water nanofluid in a circular pipe under laminar flow with wire coil inserts." Experimental Thermal and Fluid Science 34, no. 2 (2010): 122-130.
27. Pantzali, M. N., A. G. Kanaris, K. D. Antoniadis, A. A. Mouza, and S. V. Paras. "Effect of nanofluids on the performance of a miniature plate heat exchanger with modulated surface." International Journal of Heat and Fluid Flow 30, no. 4 (2009): 691-699.
28. Farajollahi, B., S. Gh Etemad, and M. Hojjat. "Heat transfer of nanofluids in a shell and tube heat exchanger." International Journal of Heat and Mass Transfer 53, no. 1-3 (2010): 12-17.
29. Shahrul, I. M., I. M. Mahbubul, R. Saidur, S. S. Khaleduzzaman, M. F. M. Sabri, and M. M. Rahman. "Effectiveness study of a shell and tube heat exchanger operated with nanofluids at different mass flow rates." Numerical Heat Transfer, Part A: Applications 65, no. 7 (2014): 699-713.
30. Lotfi, Roghayeh, Ali Morad Rashidi, and Azadeh Amrollahi. "Experimental study on the heat transfer enhancement of MWNT-water nanofluid in a shell and tube heat exchanger." International communications in heat and mass transfer 39, no. 1 (2012): 108-111.
31. Yan, Xiaoyu, Sarah Ward, David Butler, and Bébhinn Daly. "Performance assessment and life cycle analysis of potable water production from harvested rainwater by a decentralized system." Journal of Cleaner Production 172 (2018): 2167-2173.
32. Haddad, Zoubida, Chérifa Abid, Hakan F. Oztop, and Amina Mataoui. "A review on how the researchers prepare their nanofluids." International Journal of Thermal Sciences 76 (2014): 168-189.
33. Said, Zit, Rahman Saidur, M. A. Sabiha, N. A. Rahim, and M. R. Anisur. "Thermophysical properties of Single Wall Carbon Nanotubes and its effect on exergy efficiency of a flat plate solar collector." Solar Energy 115 (2015): 757-769.
34. Chang, H., Y. C. Wu, X. Q. Chen, and M. J. Kao. "Fabrication of Cu based nanofluid with superior dispersion." National Taipei University of Technology Journal 5 (2000): 201-208.
35. Pak, Bock Choon, and Young I. Cho. "Hydrodynamic and heat transfer study of dispersed fluids with submicron metallic oxide particles." Experimental Heat Transfer an International Journal 11, no. 2 (1998): 151-170.
36. Yu, Wei, Huaqing Xie, Lifei Chen, and Yang Li. "Investigation of thermal conductivity and viscosity of ethylene glycol based ZnO nanofluid." Thermochimica Acta 491, no. 1-2 (2009): 92-96.
37. 37.Correa, Daniel J., and Jacinto L. Marchetti. "Dynamic simulation of shell-and-tube heat exchangers." Heat transfer engineering 8, no. 1 (1987): 50-59.
38. Hamilton, R. L㎡, and O. K. Crosser. "Thermal conductivity of heterogeneous two-component systems." Industrial & Engineering chemistry fundamentals 1, no. 3 (1962): 187-191.
39. Murshed, S. M. S., K. C. Leong, and C. Yang. "Enhanced thermal conductivity of TiO2—water based nanofluids." International Journal of thermal sciences 44, no. 4 (2005): 367-373.
40. Yu, W., and S. U. S. Choi. "The role of interfacial layers in the enhanced thermal conductivity of nanofluids: a renovated Maxwell model." Journal of nanoparticle research 5 (2003): 167-171.
41. Timofeeva, Elena V., Alexei N. Gavrilov, James M. McCloskey, Yuriy V. Tolmachev, Samuel Sprunt, Lena M. Lopatina, and Jonathan V. Selinger. "Thermal conductivity and particle agglomeration in alumina nanofluids: experiment and theory." Physical Review E 76, no. 6 (2007): 061203.

42. Batchelor, G. K. "The effect of Brownian motion on the bulk stress in a suspension of spherical particles." Journal of fluid mechanics 83, no. 1 (1977): 97-117.
43. Drew, Donald A., and Stephen L. Passman. Theory of multicomponent fluids. Vol. 135. Springer Science & Business Media, 2006.
44. Brinkman, Hendrik C. "The viscosity of concentrated suspensions and solutions." The Journal of chemical physics 20, no. 4 (1952): 571-571.
45. Wang, Xinwei, Xianfan Xu, and Stephen US Choi. "Thermal conductivity of nanoparticle-fluid mixture." Journal of thermophysics and heat transfer 13, no. 4 (1999): 474-480.
46. Yu, Aiping, Palanisamy Ramesh, Mikhail E. Itkis, Elena Bekyarova, and Robert C. Haddon. "Graphite nanoplatelet− epoxy composite thermal interface materials." The Journal of Physical Chemistry C 111, no. 21 (2007): 7565-7569.
47. Jiang, Haifeng, Hui Li, Cheng Zan, Fuqiang Wang, Qianpeng Yang, and Lin Shi. "Temperature dependence of the stability and thermal conductivity of an oil-based nanofluid." Thermochimica Acta 579 (2014): 27-30.
48. Halelfadl, Salma, Thierry Maré, and Patrice Estellé. "Efficiency of carbon nanotubes water based nanofluids as coolants." Experimental Thermal and Fluid Science 53 (2014): 104-110.
49. Luna, Ismat Zerin, AM Sarwaruddin Chowdhury, M. A. Gafur, and Ruhul A. Khan. "Measurement of forced convective heat transfer coefficient of low volume fraction CuO-PVA nanofluids under laminar flow condition." Am. J. Nanomater 3, no. 2 (2015): 64-67.
50. Barzegarian, Ramtin, Alireza Aloueyan, and Tooraj Yousefi. "Thermal performance augmentation using water based Al2O3-gamma nanofluid in a horizontal shell and tube heat exchanger under forced circulation." International Communications in Heat and Mass Transfer 86 (2017): 52-59.
51. Damian, C. S., Devarajan, Y., Raja, T., & Jayabal, R. (2024). A comprehensive review of biomass pyrolysis for hydrogen production in India. Process Safety and Environmental Protection, 190, 646–662. https://doi.org/10.1016/j.psep.2024.07.034
52. Muralidaran, V. M., Natrayan, L., Kaliappan, S., & Patil, P. P. (2024). Grape stalk cellulose toughened plain weaved bamboo fiber-reinforced epoxy composite: load bearing and time-dependent behavior. Biomass Conversion and Biorefinery, 14(13), 14317-14324.
53. Sathish, T., Saravanan, R., Giri, J., Al-Kahtani, A. A., Prakash, C., Kumar, A., ... & Ubaidullah, M. (2024). Hydrogen conversion by microalgae through water gasification under different operating conditions, and Fe2O3, Al2O3, and CaO additives: An experimental study. International Journal of Hydrogen Energy.
54. Yu, Wenhua, David M. France, David S. Smith, Dileep Singh, Elena V. Timofeeva, and Jules L. Routbort. "Heat transfer to a silicon carbide/water nanofluid." International Journal of Heat and Mass Transfer 52, no. 15-16 (2009): 3606-3612.
55. Kumar, NT Ravi, P. Bhramara, A. Kirubeil, L. Syam Sundar, Manoj K. Singh, and Antonio CM Sousa. "Effect of twisted tape inserts on heat transfer, friction factor of Fe3O4 nanofluids flow in a double pipe U-bend heat exchanger." International Communications in Heat and Mass Transfer 95 (2018): 53-62.
56. Balaji, K., S. Iniyan, and Muthusamy V. Swami. "Exergy, economic and environmental analysis of forced circulation flat plate solar collector using heat transfer enhancer in riser tube." Journal of Cleaner Production 171 (2018): 1118-1127.
57. Bahiraei, Mehdi, Reza Rahmani, Ali Yaghoobi, Erfan Khodabandeh, Ramin Mashayekhi, and Mohammad Amani. "Recent research contributions concerning use of nanofluids in heat exchangers: a critical review." Applied Thermal Engineering 133 (2018): 137-159.
58. Kannadasan, N., K. Ramanathan, and S. Suresh. "Comparison of heat transfer and pressure drop in horizontal and vertical helically coiled heat exchanger with CuO/water based nano fluids." Experimental Thermal and Fluid Science 42 (2012): 64-70.
59. Kumar, NT Ravi, P. Bhramara, A. Kirubeil, L. Syam Sundar, Manoj K. Singh, and Antonio

CM Sousa. "Effect of twisted tape inserts on heat transfer, friction factor of Fe3O4 nanofluids flow in a double pipe U-bend heat exchanger." International Communications in Heat and Mass Transfer 95 (2018): 53-62.

60. J. Kumaraswamy et al., "Thermal Analysis of Ni-Cu Alloy Nanocomposites Processed by Sand Mold Casting," Advances in Materials Science and Engineering, vol. 2022, Article ID 2530707, 11 pages, 2022. https://doi.org/10.1155/2022/2530707.
61. Raja, T., Raja, K. V., Reddy, M. I., Al Obaid, S., Alharbi, S. A., & Kalam, M. A. (2023). Studies on mechanical and morphological behaviors of banyan/kevlar fibers reinforced MgO particulates hybrid aliphatic epoxy composite. The International Journal of Advanced Manufacturing Technology, 1-8. https://doi.org/10.1007/s00170-023-11852-w
62. Khatoon, Umme Thahira, and Aditya Velidandi. "Silver oxide nanoparticles: Synthesis via chemical reduction, characterization, antimicrobial, and cytotoxicity studies." Inorganic Chemistry Communications 159 (2024): 111690. https://doi.org/10.1016/j.inoche.2023.111690